Supporting Information

Stabilization Effects in Binary Colloidal Cu and Ag Nanoparticle Electrodes under Electrochemical CO_2 Reduction Conditions

Longfei Wu,[a] Kees E. Kolmeijer,[a] Yue Zhang,[b] Hongyu An,[a] Sven Arnouts,[c,e] Sara Bals,[c] Thomas Altantzis,[e] Jan P. Hofmann,[d] Marta Costa Figueiredo,[b] Emiel J.M. Hensen,[b] Bert M. Weckhuysen,[a] and Ward van der Stam*[a]

*Email address of corresponding author: w.vanderstam@uu.nl

---

[a] Inorganic Chemistry and Catalysis group, Institute for Sustainable and Circular Chemistry, Utrecht University, 3584 CG Utrecht, The Netherlands. Email: w.vanderstam@uu.nl

[b] Laboratory for Inorganic Materials and Catalysis, Department of Chemical Engineering and Chemistry, Eindhoven University of Technology, 5600 MB Eindhoven, The Netherlands.

[c] Electron Microscopy for Materials Research (EMAT), University of Antwerp, 2020 Antwerp Belgium.

[d] Surface Science Laboratory, Department of Materials and Earth Sciences, Technical University of Darmstadt, 64287 Darmstadt, Germany

[e] Applied Electrochemistry & Catalysis (ELCAT), University of Antwerp, 2610 Wilrijk, Belgium

Table of Contents

Part I: Experimental details

Cu nanoparticles (NPs) synthesis: Cu NPs were synthesized via decomposition of copper(I) acetate (CuOAc) in trioctylamine (TOA) in the presence of tetradecylphosphonic acid (TDPA) and oleic acid following an adaptation of a reported method.[1] Specifically, 10 mL TOA was added into a 100 mL three neck flask containing 10 mL 1-octadecene and equipped with a condenser, a glass stir bar and a thermocouple inserted in a 1-octadecene filled glass tube. Afterwards, 123 mg CuOAc (1 mmol), 278 mg TDPA (1 mmol) and 0.7 mL oleic acid (2.22 mmol) were added to the TOA accordingly. The solution was firstly heated at 100 °C for an hour under vacuum and then quickly heated to 180 °C under Ar or N_2 flow and maintained at 180 °C for 30 mins. Eventually, the solution was heated to 220 °C and kept for 30 mins. The red colloidal solution was cooled to room temperature with an air gun, and the copper NPs were removed using air-free techniques through a purged syringe and stored in a nitrogen filled glovebox. To wash the excess reactants, the colloidal NPs were precipitated with a 1:1 ratio of colloidal solution with ethanol. Afterwards, the mixture was centrifuged at 3000 rpm for 5 mins. After removing the supernatant, the NPs were re-dispersed in hexane.

Ag NPs synthesis: Ag NPs were prepared by decomposition of silver nitrate ($AgNO_3$) in trioctylamine (TOA) with tetradecylphosphonic acid (TDPA) and oleic acid as surfactants. Briefly, 170 mg $AgNO_3$ and 278 mg TDPA were added into a 100 mL three-neck flask connected to a condenser and a glass stir bar. After adding 0.7 mL oleic acid, 20 mL 1-Octadecene and 1.0 ml TOA respectively, the solution was degassed for 1 h under vacuum at room temperature. Then, the mixed solution was heated to 80 °C rapidly under Ar or N_2 flow and kept at this temperature for 30 mins. Afterwards, the solution was heated to 120 °C and kept for 30 mins. Finally, the colloidal solution was cooled down to room temperature with an air gun and the Ag NPs were extracted and stored in a nitrogen filled glovebox in a similar way as described above.

Inductively coupled plasma optical emission spectrometry (ICP-OES): The concentration of the stock Cu and Ag NP solution was determined to be 0.064 and 0.026 mol/L respectively by ICP-OES, PerkinElmer Optima 8300 Optical Emission Spectrometer. Briefly, the samples were first dissolved in 68 % HNO_3, and were further diluted to 5% HNO_3 solution. Afterwards, 10 ml of the diluted solution was taken for Cu (spectral lines: 327.39, 324.75, 224.70 nm) and Ag (spectral lines: 328.06, 338.29, 243.78 nm) in ICP-OES. Calibration curves of 0, 0.2, 0.4, 0.6, 0.8 and 1.0 mg L^{-1} were prepared for both Cu and Ag. Based on ICP concentration and TEM size analysis, we calculate the nanoparticle density of Cu and Ag bulk solutions, which are 1.0437×10^{15} (Cu) and 1.8593×10^{15} per ml.

(Scanning) Transmission electron microscopy ((S)TEM): TEM images were acquired with a FEI Talos F200X transmission electron microscope equipped with a LaB_6 filament and operated at an acceleration voltage of 200 kV. High-angle annular dark field scanning transmission electron microscopy (HAADF-STEM) images and energy dispersive X-rays spectroscopy (EDXS) elemental maps were acquired using a FEI-Osiris and an aberration-corrected ‘cubed’ FEI-Titan transmission electron microscopes operated at 200 kV and 300 kV respectively, both equipped with the ChemiSTEM system.[2]

Conventional electron tomography: Electron tomography tilt series were acquired in HAADF-STEM mode using a FEI-Osiris electron microscope operated at 200 kV. For the Cu NPs a tilt range from –58° to +66° and a tilt increment of 2° were used whereas for Ag NPs, a tilt range from –70° to +76° and a tilt increment of 2° were used. The reconstruction was performed using the EM algorithm as implemented in the ASTRA Toolbox.[3]

Atomic Resolution Electron Tomography: For the acquisition of the atomic resolution tomography series, we recorded a time series of 3 images for each projection using a dwell time of 1 µs. The series were acquired within a tilt range from -76° to +76° and a tilt increment of 2° using a FEI-Titan transmission electron microscope operated at 300 kV. The correction of distortions at each image of the time series for each projection, the alignment of the series and the reconstruction of the aligned series were performed using the approach recently described from our group.[4]

Scanning electron microscopy (SEM): SEM images were acquired on a FEI Helios Nanolab G3 with accelerating voltage of 5.0 keV and probe current of 0.2 nA.

X-ray photoelectron spectroscopy (XPS): XPS spectra were recorded on a ThermoScientific K-Alpha spectrometer Al Kα (1486.6 eV). The spectra were fitted by CasaXPS software using a Shirley background subtraction, Doniach-Sunjic (DS) line-shape (DS (0.001, 250)) for Cu^0 and Gaussian (70%)-Lorentzian (30%) line shape for other components. Survey scans were collected at constant pass energy of 200 eV and region scans at 50 eV.

X-ray diffraction (XRD) measurements: X-ray diffraction with Bragg-Brentano configuration was recorded with a Bruker D2 PHASER diffractometer using Co Kα (1.789 Å) radiation. Grazing incidence X-ray diffraction was performed on Bruker D8 Advance with Cu Kα (1.540 Å) radiation.

Electrophoresis: Electrophoresis was conducted in a home-made two-electrode electrochemical cell with 1 cm distance between cathode and anode, and the potential was controlled by a DELTA ELEKTRONIKA SM 300-5 power supply. Due to the high voltage applied, the cell was placed in a safety box connected to an inter-lock of the power supply, and the safety box was ventilated to remove evaporated organic solvent during operation. Specifically, Cu NPs stock solution was diluted 100 times with hexane in the glovebox, then 1 mL of the diluted solution was taken out of the glovebox and added to the electrophoresis cell and set at a certain potential for 60 mins. For Cu-Ag mixed NPs film preparation, 500 µL of the diluted Cu and Ag NPs solutions was thoroughly mixed and added to the electrochemical cell for electrophoresis. The electrodes after electrophoresis were directly transferred to glovebox and dried under vacuum overnight.

Drop casting: Drop casting of nanoparticle electrodes was performed in a N_2-filled glovebox to avoid surface oxidation. Briefly, 50 µL Cu NP solution was drop casted on polished (polished by 50 nm alumina slurry and thoroughly cleaned in MilliQ water and ethanol) 1 by 1 cm glassy carbon electrode. Afterwards, the nanoparticle electrode was dried in the glovebox overnight before electrochemical tests.

CO_2 reduction reaction (CO2RR) measurements: CO2RR were carried out in a two-compartment home-made three-electrode electrochemical cell.[5] The cathode and anode chambers were separated by a cation exchange membrane (Nafion™ 115). Prior to CO_2 reduction, 0.1 M $KHCO_3$ in milli-Q water was bubbled with CO_2 for at least 20 mins and continuously purged with CO_2 during the measurements. The gas products at the cathode were directly vented into the gas-sampling loop of the gas chromatograph (Thermo Scientific TRACE 1300 Gas Chromatograph) equipped with a thermal conductivity detector (TCD) and flame ionization detector (FID) for quantification. Liquid products were determined by ^1H NMR spectroscopy with 400 MHz spectrometer (Bruker). Briefly, 450 µL electrolyte was mixed with 50 µL internal standard solution composed of 1 mM dimethyl sulfoxide (DMSO, Sigma-Aldrich, 99.9%) and 5 mM phenol (Sigma-Aldrich, 99.0-100.5%) in D_2O (Sigma-Aldrich, 99.9 at. % D). The mixture was transferred to NMR sample tube and analyzed by NMR spectrometer.

Part II: Characterization

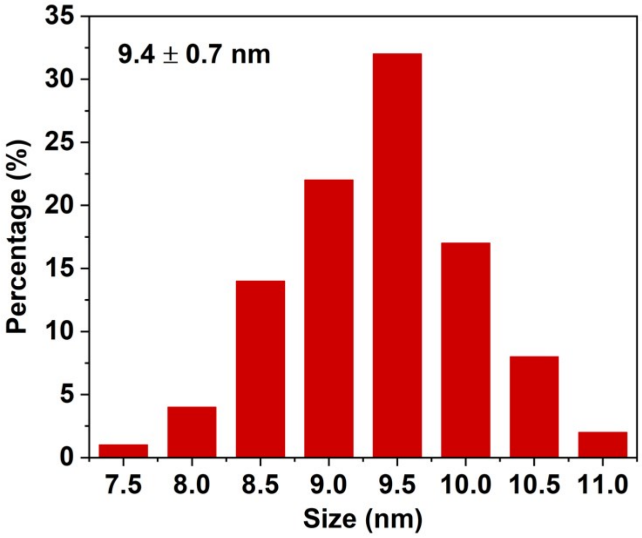

Figure S1. Size histogram of as-synthesized colloidal Cu NPs (100 nanoparticles were counted).

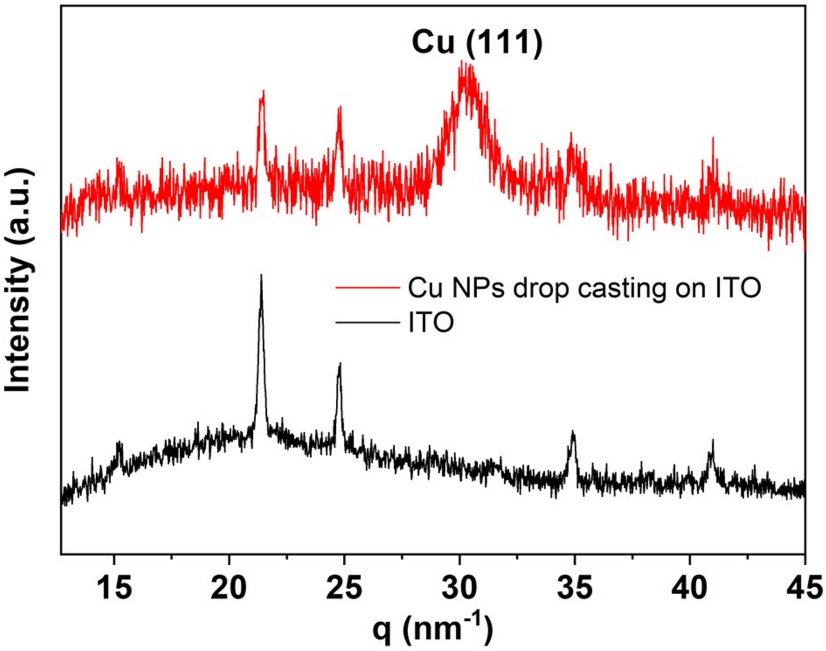

Figure S2. X-ray diffraction pattern of colloidal Cu nanoparticles on an ITO substrate.

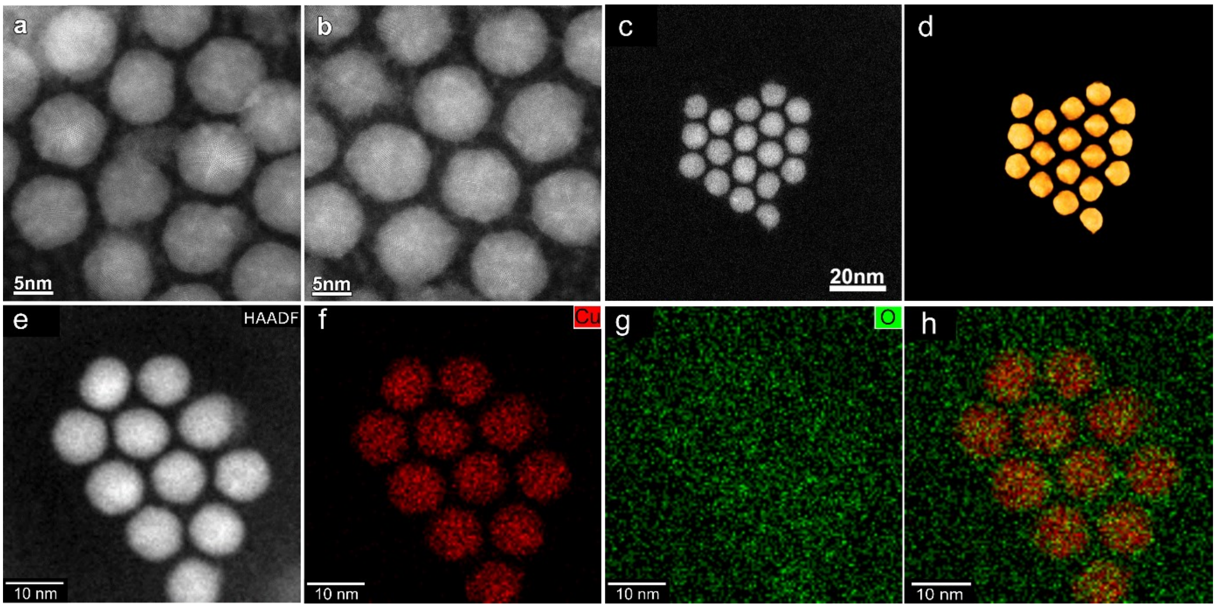

Figure S3. High resolution HAADF-STEM images of the colloidal Cu NPs (a, b). HAADF-STEM image (c) and reconstructed volume of Cu NPs (d). (e-h) HAADF-STEM image and the corresponding elemental EDXS maps of copper and oxygen.

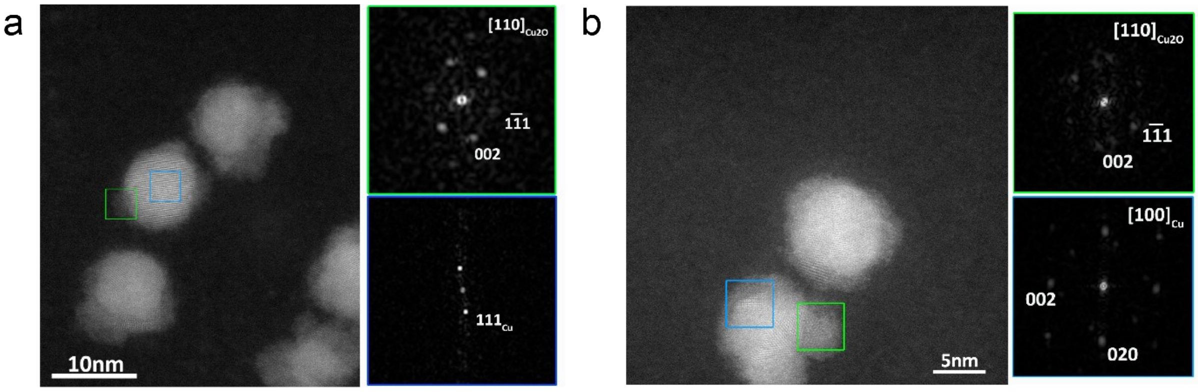

Figure S4. High resolution HAADF-STEM images and respective FT analysis of Cu NPs after exposure to air for 3 hours.

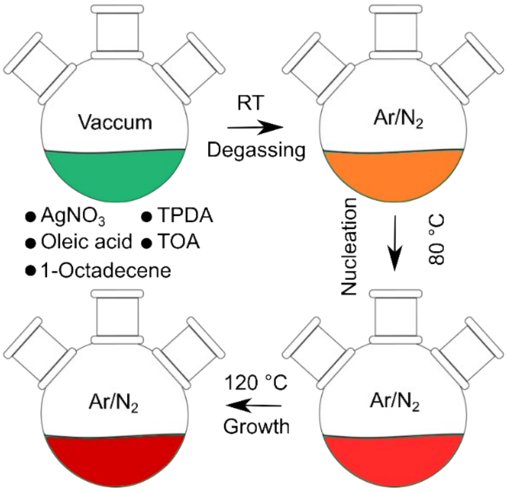

Figure S5. Synthetic scheme of colloidal Ag NPs.

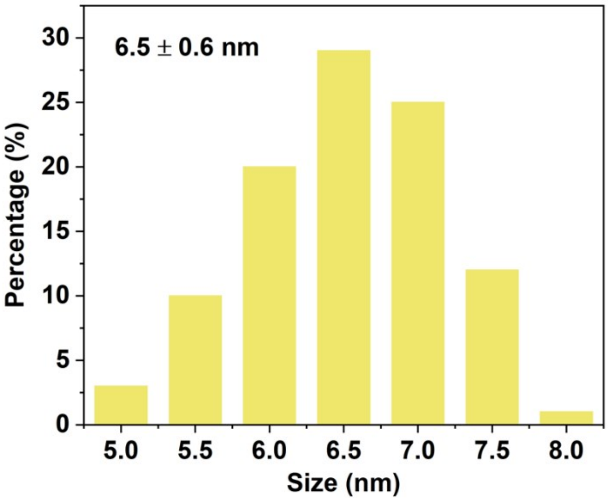

Figure S6. Size histogram of colloidal Ag NPs (100 nanoparticles were counted).

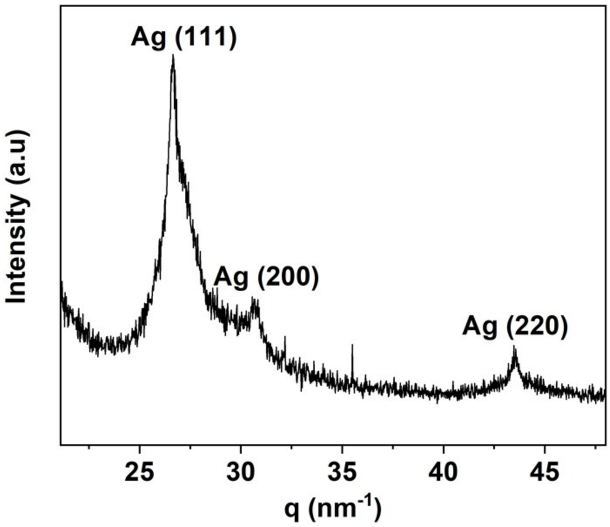

Figure S7. Grazing incidence X-ray diffraction pattern of colloidal Ag nanoparticles on a glassy carbon electrode (angle of incidence 0.5°).

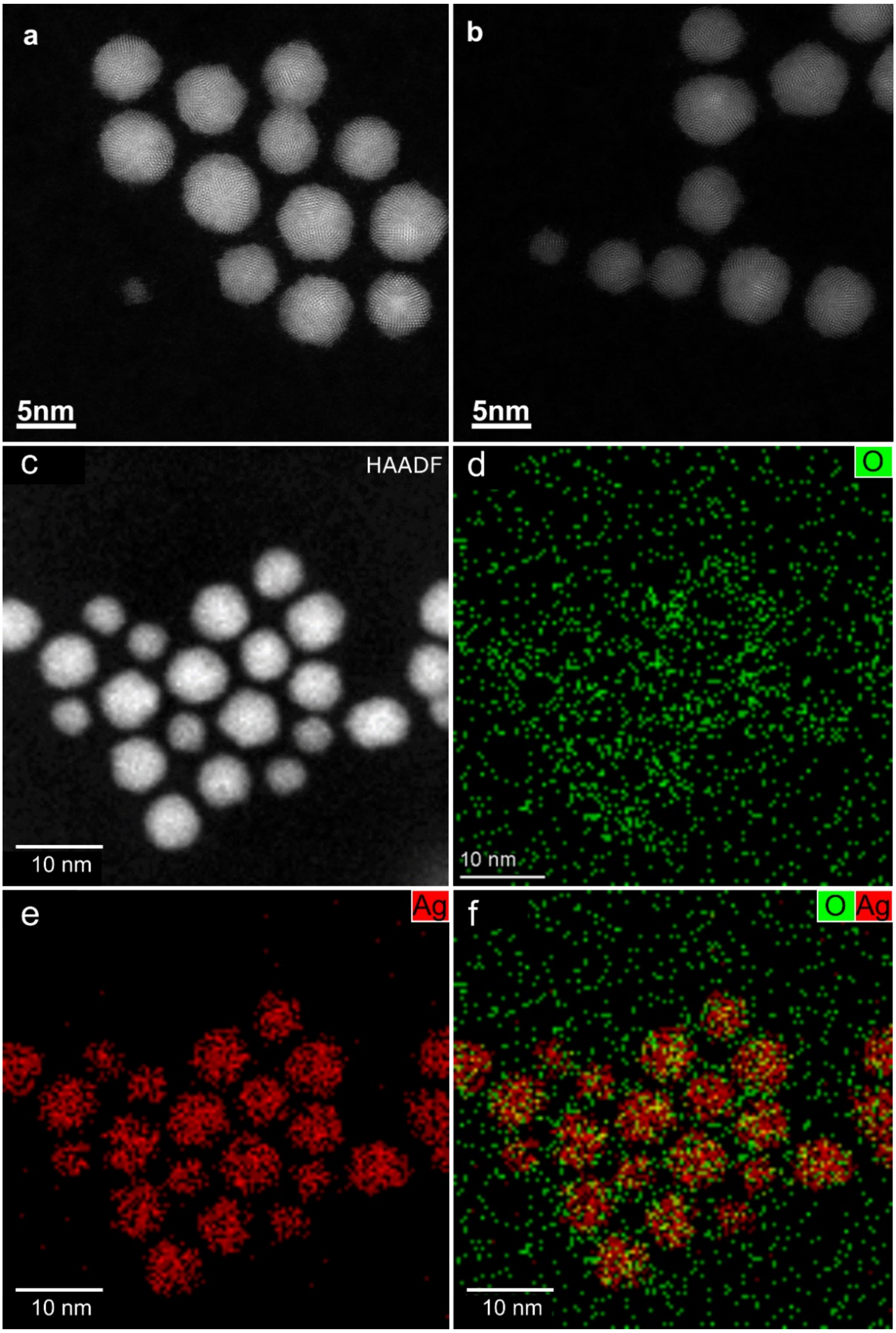

Figure S8. STEM-HAADF images (a-c) of Ag NPs, and the corresponding elemental EDXS (d-f) maps for silver and oxygen.

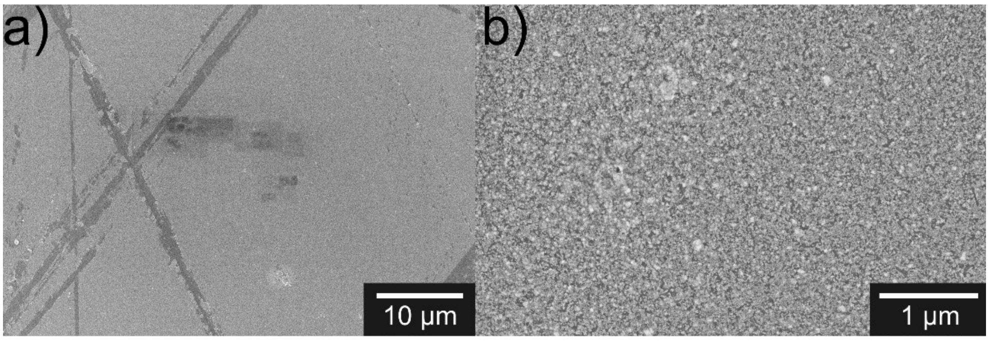

Figure S9. SEM images of Cu NPs film prepared via electrophoresis at the anode (100 V-60 mins).

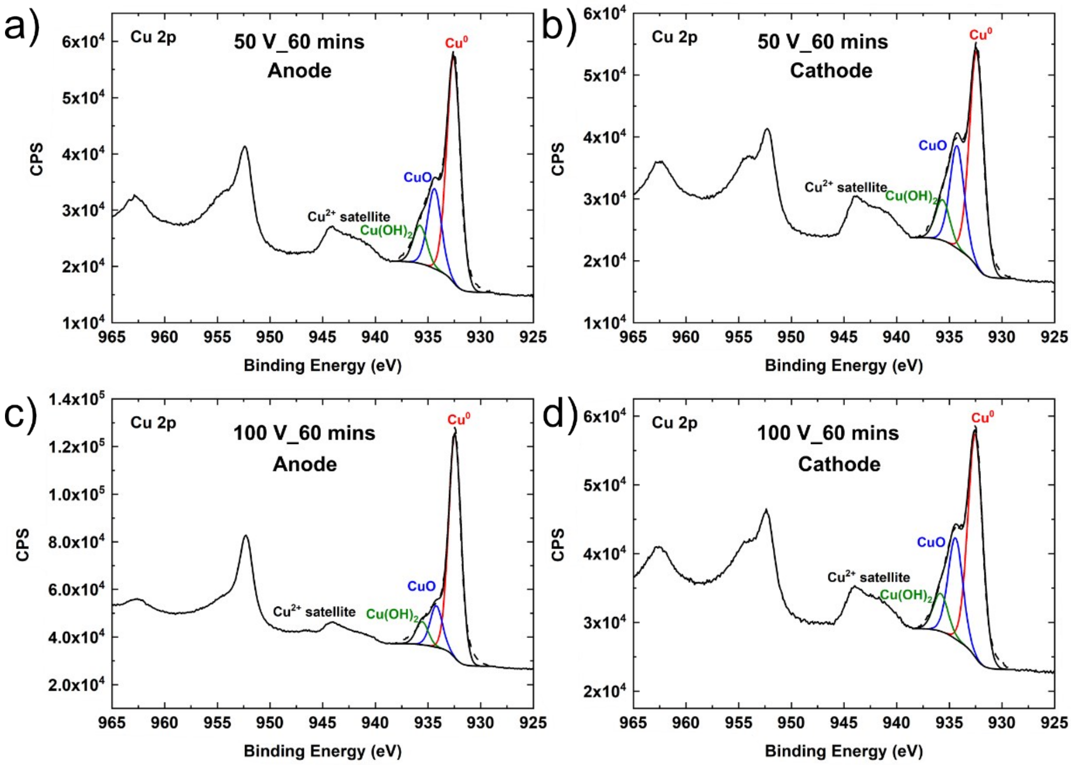

Figure S10. XPS spectra of Cu NP films prepared by electrophoresis at 50 V (a, b) and 100 V (c, d) respectively, showing more severe oxidation at the cathode films.

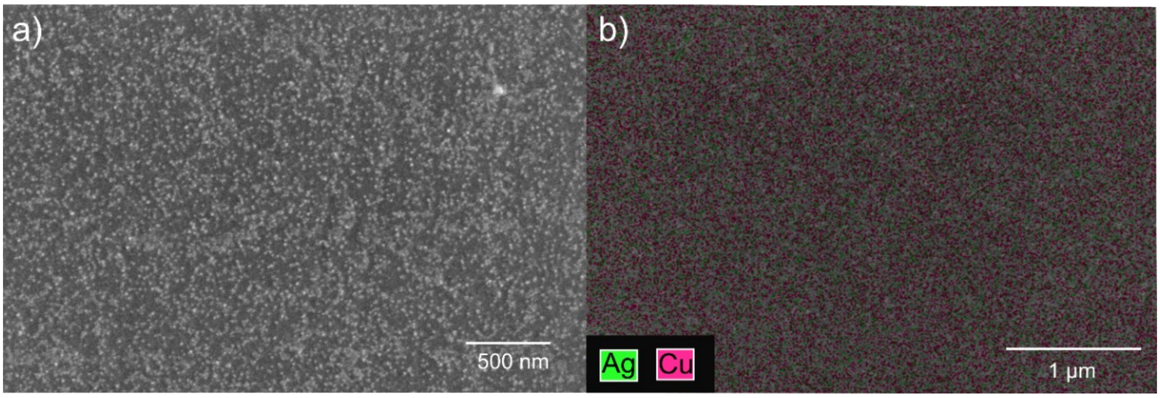

Figure S11. SEM image (a) and EDXS mapping (b) of as-prepared Cu-Ag film.

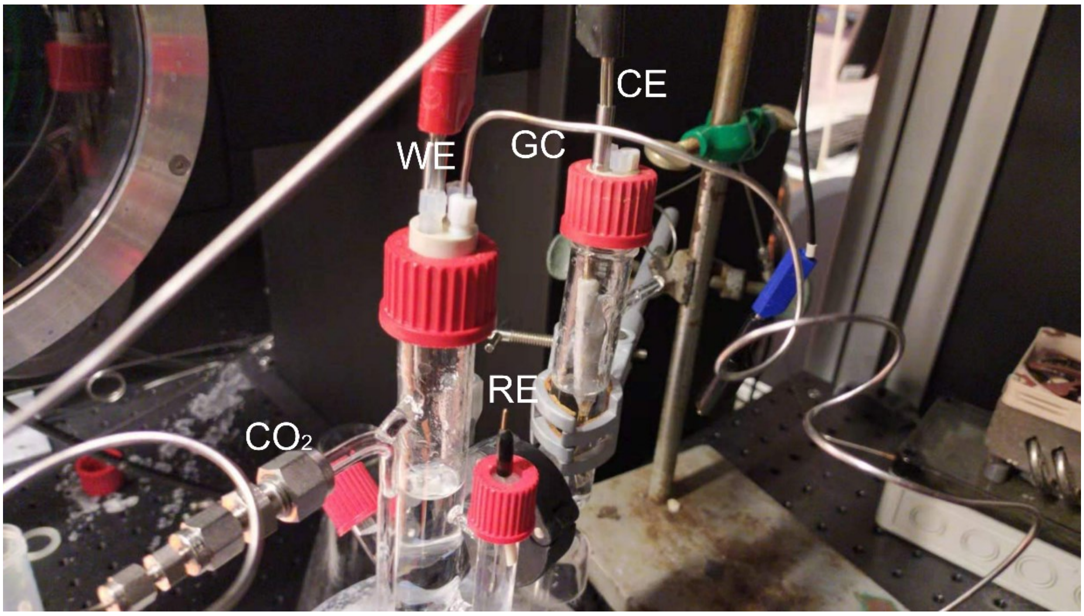

Figure S12. Photograph of CO2RR activity measurement setup and electrochemical cell.

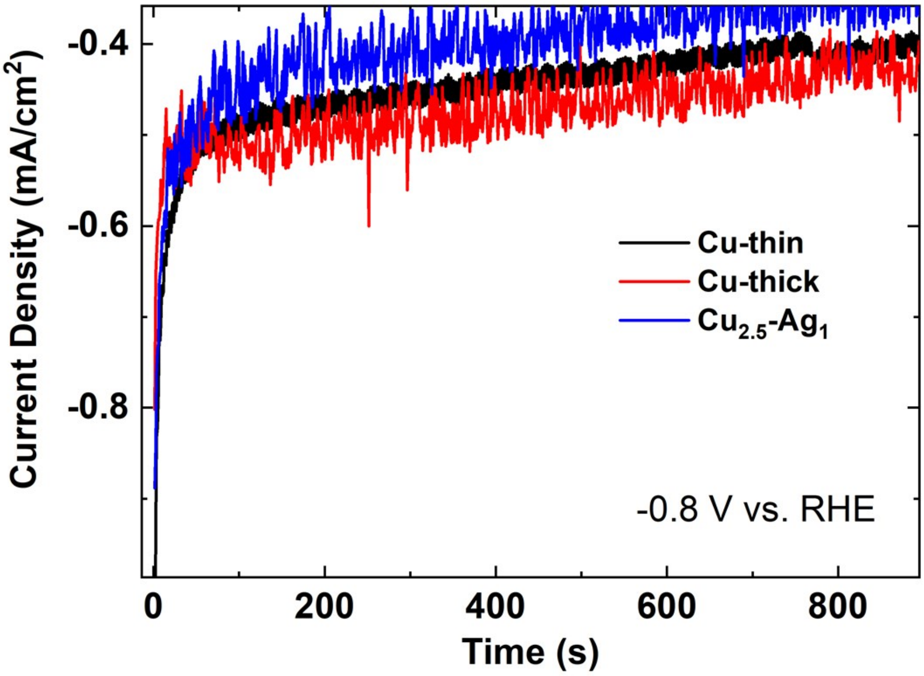

Figure S13. Zoom-in chronoamperometry curves of Cu NP and $Cu_{2.5}$-Ag_1 films recorded at -0.8 V vs. RHE in CO_2 saturated 0.1 M $KHCO_3$ aqueous electrolyte solution.

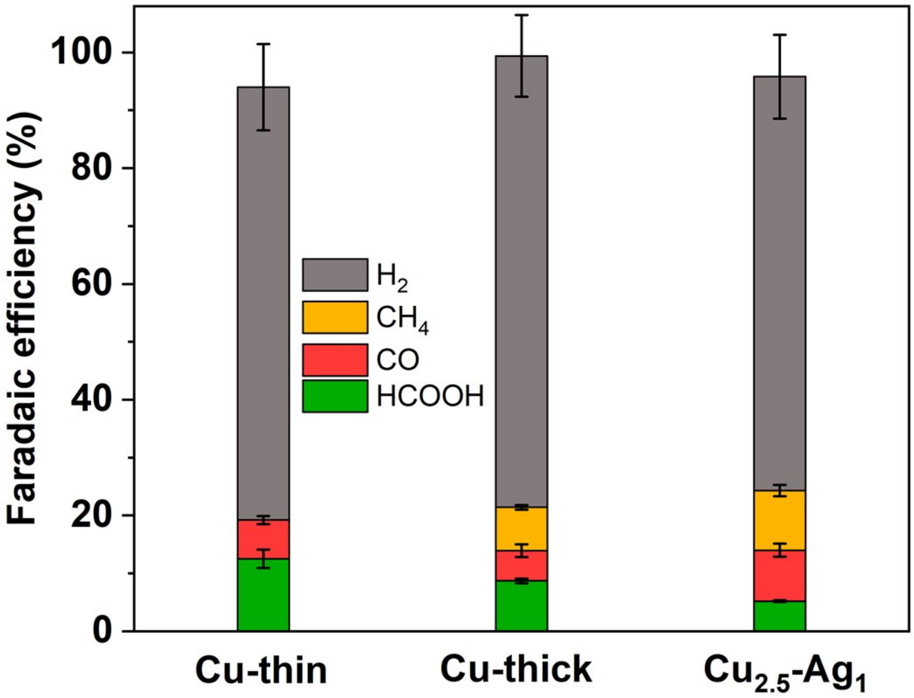

Figure S14. Faradaic efficiency of Cu-Ag NP films for CO2RR and HER at -0.8 V vs. RHE in CO_2 saturated 0.1 M $KHCO_3$.

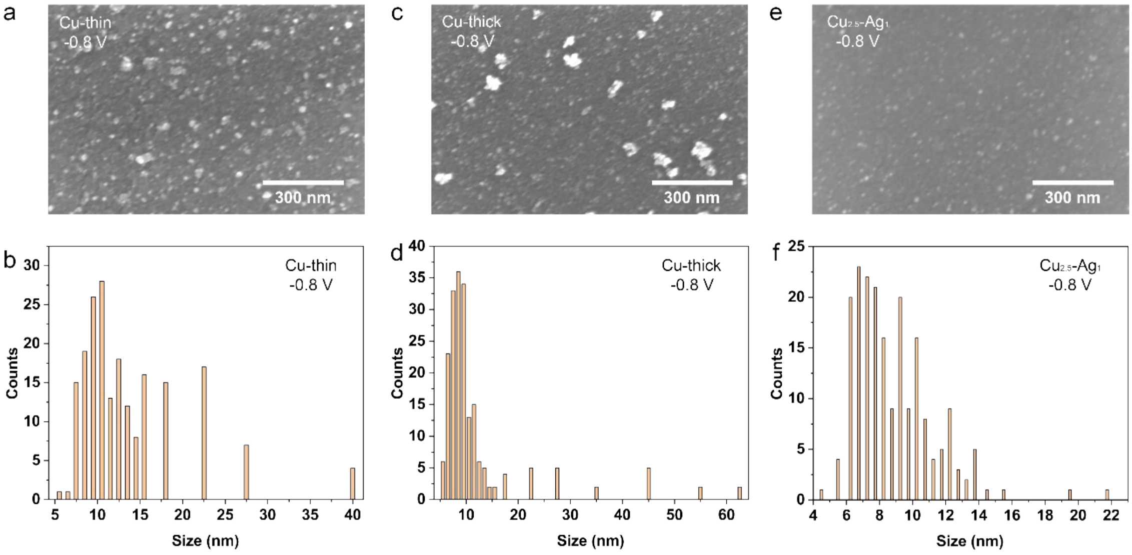

Figure S15. High resolution SEM images (a, c, e) and the corresponding particle size distribution analysis (b, d, f). 200 particles were counted for each SEM image.

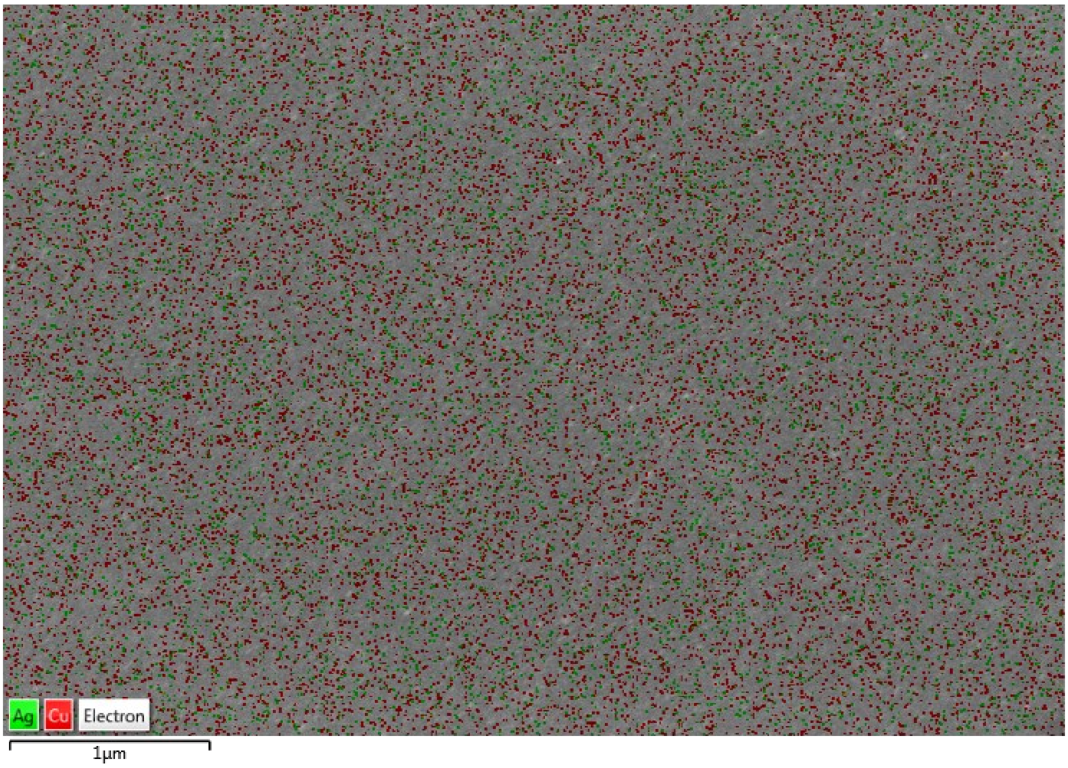

Figure S16. EDXS mapping of Cu and Ag element for Cu$_{2.5}$-Ag$_1$ after CO2RR at -0.8 V *vs.* RHE for 1h.

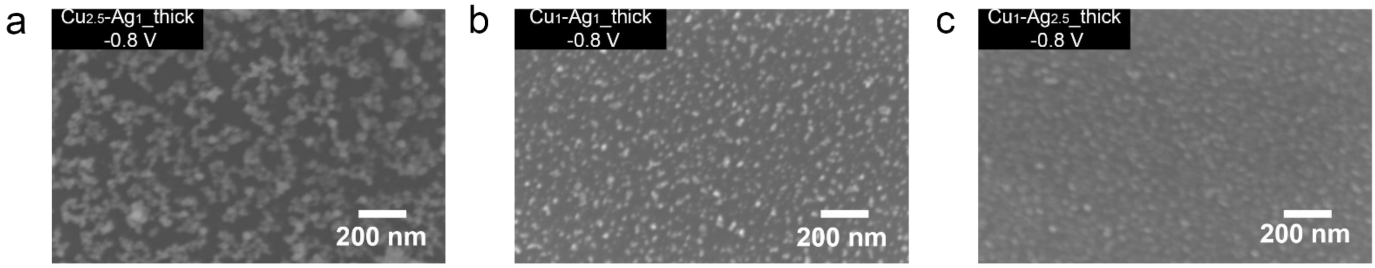

Figure S17. High resolution SEM images of Cu$_{2.5}$-Ag$_1$_thick (a), Cu$_1$-Ag$_1$_thick (b) and Cu$_1$-Ag$_{2.5}$_thick (c) after CO2RR at -0.8 V vs. RHE for 1 h.

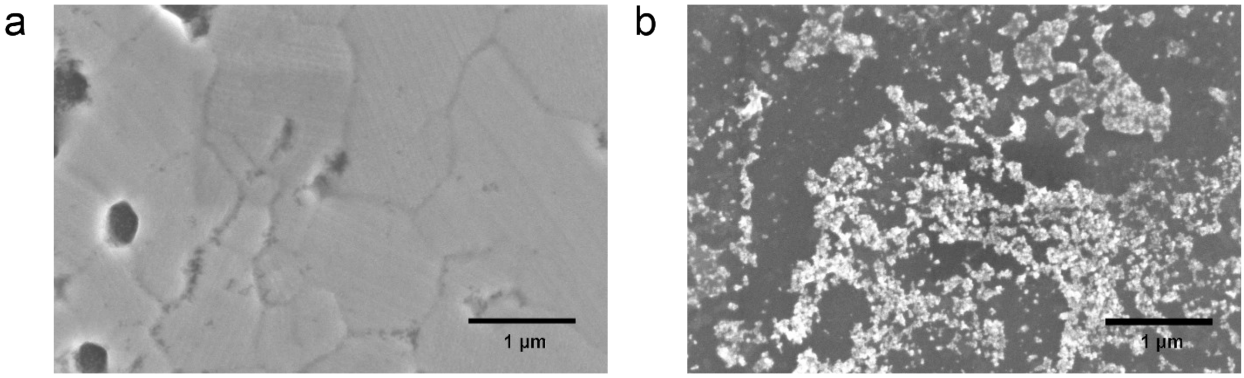

Figure S18. SEM images of drop casted pristine Cu NP film (a) and that after CO2RR -1.2 V (d) vs. RHE for 1 h in CO$_2$ saturated 0.1 M KHCO$_3$.

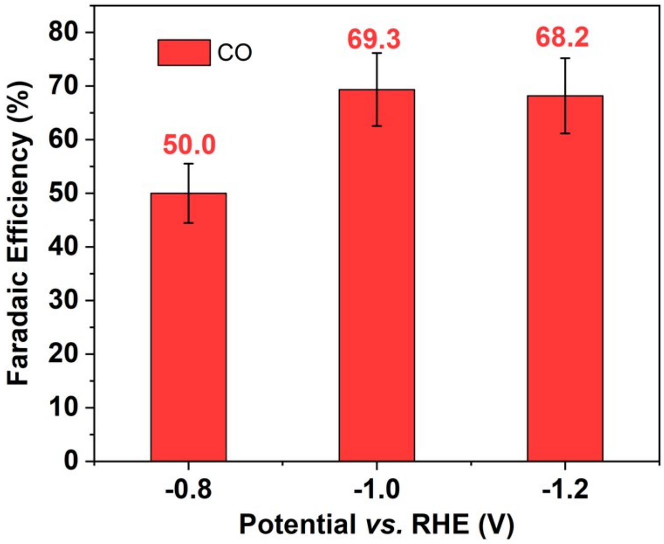

Figure S19. Faradaic efficiency of drop casted Ag NP films for CO2RR at -0.8 V, -1.0 V, -1.2 V vs. RHE for 1 h in CO_2 saturated 0.1 M $KHCO_3$.

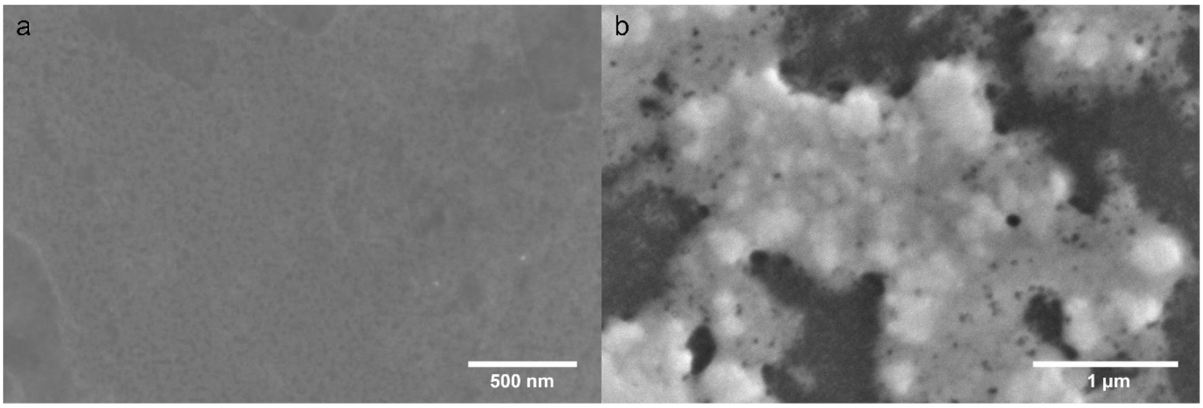

Figure S20. SEM images of pristine drop casted Ag (a) and Cu-Ag (b) NP films.

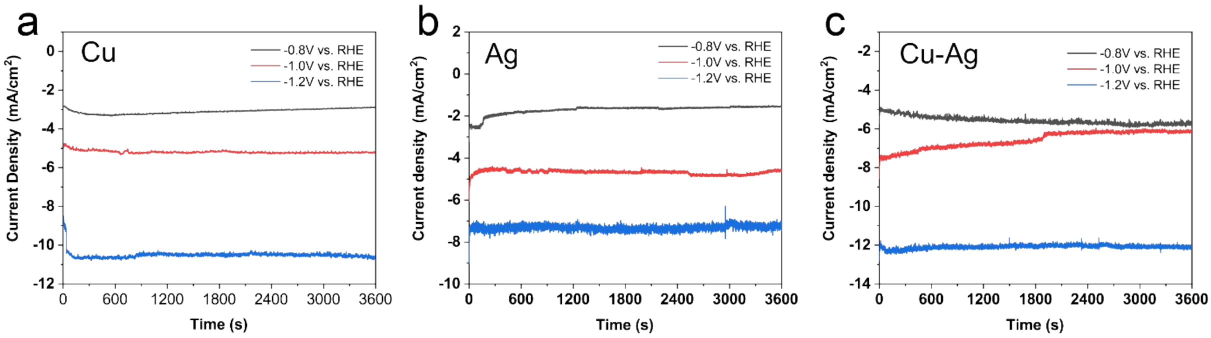

Figure S21. Chronoamperometry curves of drop casted NP films during CO2RR in CO_2 saturated 0.1 M $KHCO_3$ aqueous electrolyte solution.

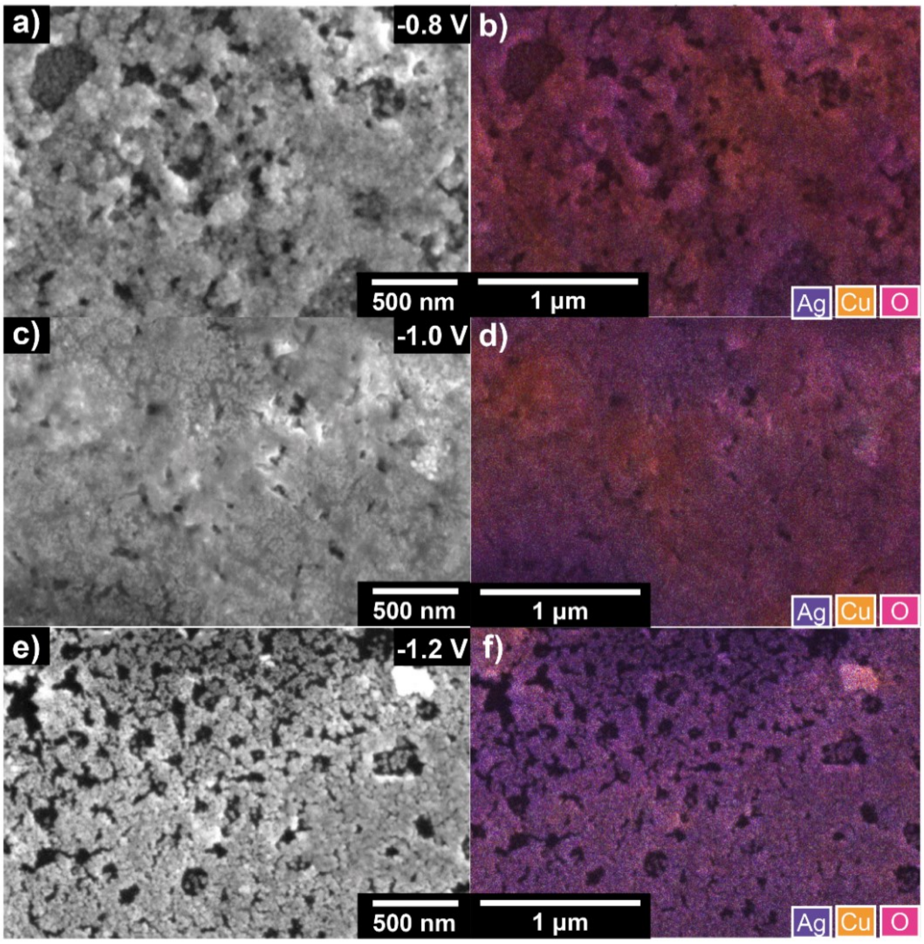

Figure S22. SEM (a, c) images and the corresponding EDS mappings (b, d) of $Cu_{1.0}$_$Ag_{1.0}$ films after CO2RR at -0.8 V, -1.0 V and -1.2 V vs. RHE for 1 h. For EDXS mapping, Orange and purple corresponds to Cu and Ag respectively.

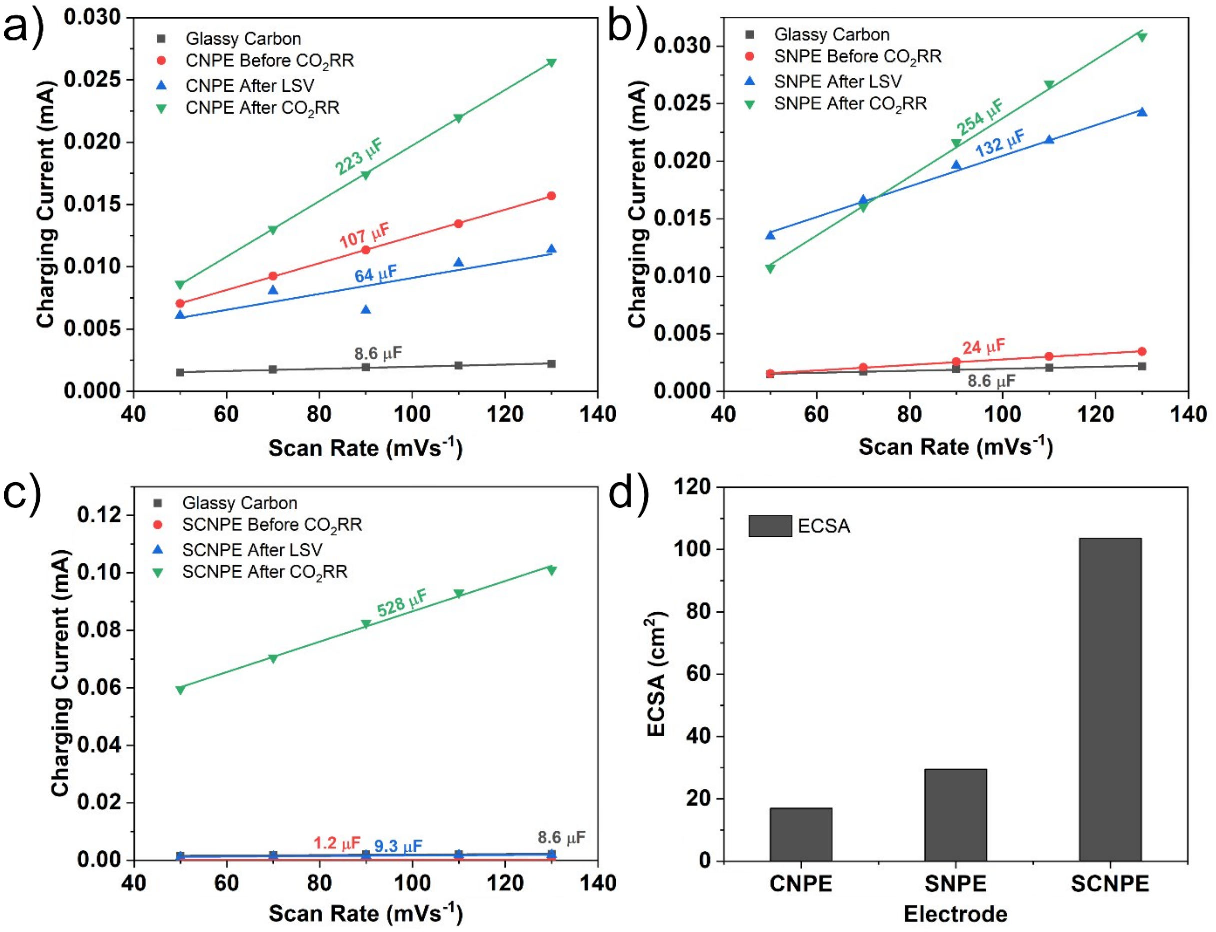

Figure S23. Electrochemical double layer capacitance measurements for (a) Cu NP electrode (CNPE), (b) Ag NP electrode (SNPE) and (c) Cu-Ag NP electrode (CSNPE), and (d) the corresponding electrochemical surface area (ECSA) determination.

ECSA calculation

The electrochemical surface area (ECSA) was determined from

(1) $R_f = C / C_S$
(2) $ECSA = R_f * S$

Were Rf is the roughness factor, C is the Double Layer Capacitance of the sample ($F = A^2\, s^4\, kg^{-1}\, m^{-2}$) and C_S is the Double Layer Capacitance of the substrate (glassy carbon), and S is the geometric surface area (1.0 cm^2). C is obtained from the slope of a linear fit of the charging current measured at varying scan rates in a non-faradaic region of the cyclic voltammograms.

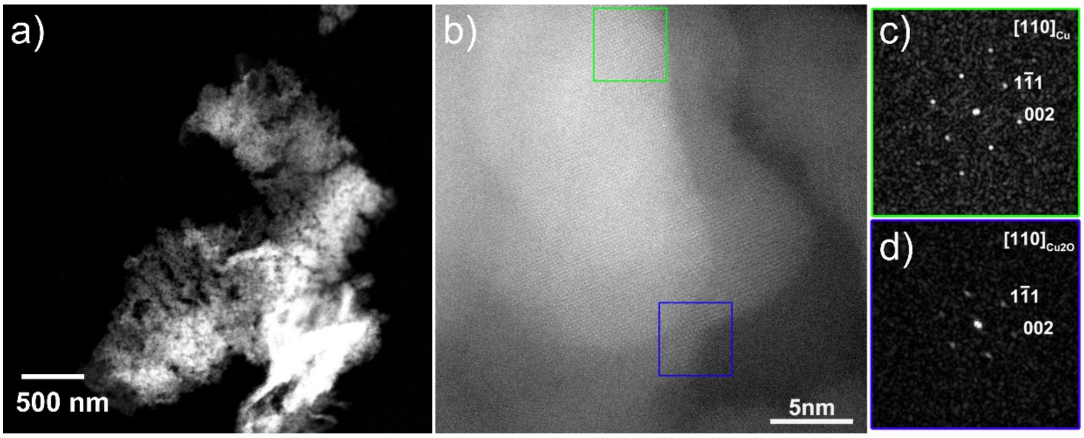

Figure S24. a) Low magnification HAADF-STEM image of drop casted Cu NP electrode after CO2RR at -1.0 V vs. RHE for 1 h. b-d) High magnification HAADF-STEM image of (a) showing that both metallic Cu and Cu_2O regions are present.

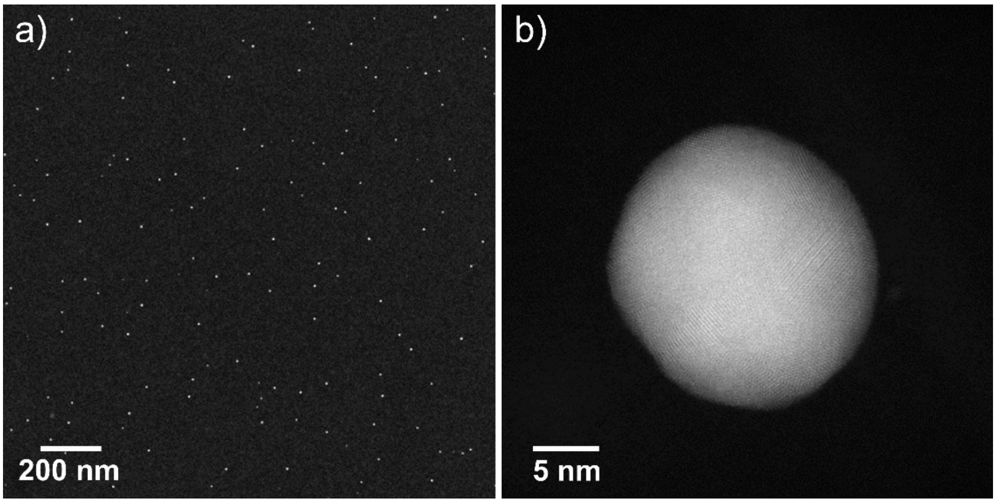

Figure S25. a) Low magnification HAADF-STEM image of drop casted Cu-Ag NP electrode after CO2RR at -0.8 V vs. RHE for 1 h. b) High magnification HAADF-STEM image of one of the individual NPs corresponding to that of metallic Ag.

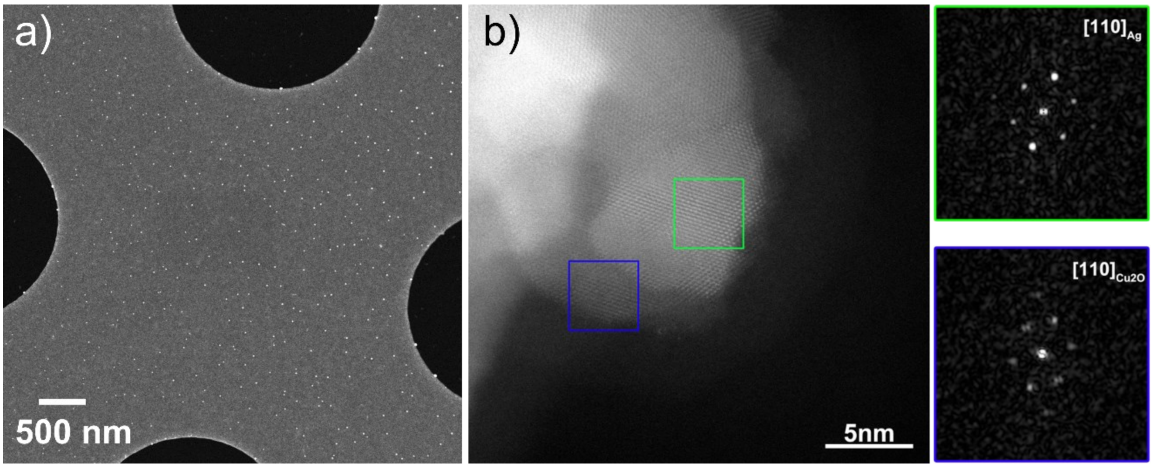

Figure S26. a) Low magnification HAADF-STEM image of drop casted Cu-Ag NP electrode after CO2RR at -1.0 V vs. RHE for 1 h. b) High magnification HAADF-STEM image showing that both metallic Ag and Cu_2O regions are present.

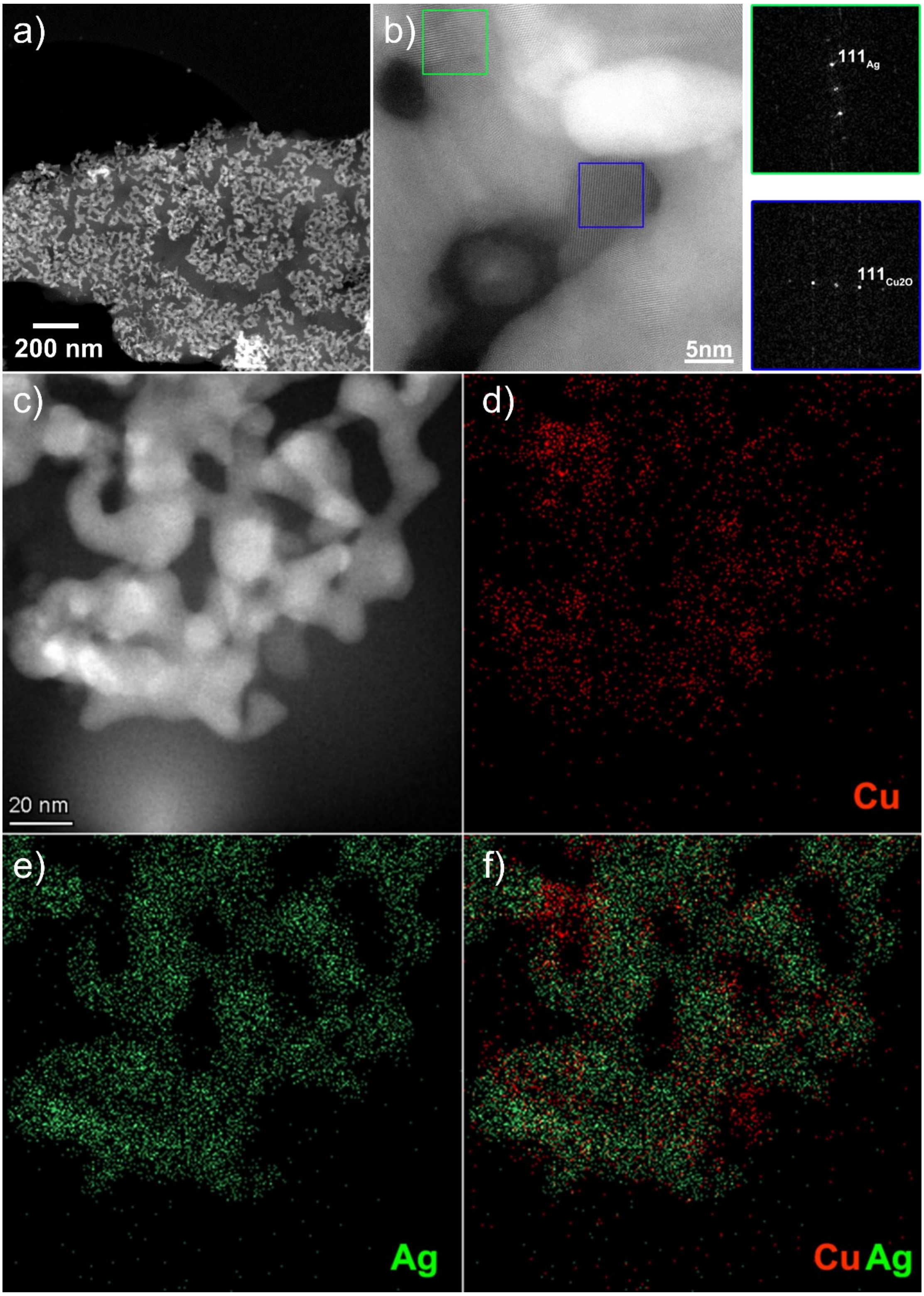

Figure S27. a) Low magnification HAADF-STEM image of drop casted Cu-Ag NP electrode after CO2RR at -1.2 V vs. RHE for 1 h. b) High magnification HAADF-STEM image from a region of an agglomerated network. It is clear that both metallic Ag and Cu_2O regions are present. c-f) HAADF-STEM image and the corresponding EDXS elemental maps of Cu and Ag. It can be seen that there are regions where it seems that the two elements are mixed but most of them are separated.

1. K. Manthiram, B. J. Beberwyck and A. P. Alivisatos, *J Am Chem Soc*, 2014, **136**, 13319-13325.
2. P. Schlossmacher, D. O. Klenov, B. Freitag and H. S. von Harrach, *Microscopy Today*, 2010, **18**, 14-20.
3. W. van Aarle, W. J. Palenstijn, J. De Beenhouwer, T. Altantzis, S. Bals, K. J. Batenburg and J. Sijbers, *Ultramicroscopy*, 2015, **157**, 35-47.
4. T. Milagres de Oliveira, W. Albrecht, G. Gonzalez-Rubio, T. Altantzis, I. P. Lobato Hoyos, A. Beche, S. Van Aert, A. Guerrero-Martinez, L. M. Liz-Marzan and S. Bals, *ACS Nano*, 2020, **14**, 12558-12570.
5. K. Liu, M. Ma, L. Wu, M. Valenti, D. Cardenas-Morcoso, J. P. Hofmann, J. Bisquert, S. Gimenez and W. A. Smith, *ACS Appl Mater Interfaces*, 2019, **11**, 16546-16555.